



In Situ Polymerization and Characterization of PANI/CoFe₂O₄ Nanocomposites for Thermal, Magnetic, Electrical, and Electrochemical Properties

Swati¹ · Monika Saini¹ · Anupama¹ · Rajni Shukla¹ · Vikram² · Prakash Chand³

Received: 14 February 2023 / Accepted: 10 March 2023 / Published online: 12 April 2023

© The Author(s), under exclusive licence to Springer Science+Business Media, LLC, part of Springer Nature 2023

Abstract

Composites of polyaniline and cobalt ferrite have been prepared using in-situ chemical polymerization to study their supercapacitive behaviour with electrical, thermal, and magnetic properties in light of the progressing applications of conducting polymers. X-ray diffraction and Fourier transform infrared spectroscopy were used to confirm the synthesis of materials and to carry out their structural studies. Scanning electron microscope image clears the embeddedness of nanoparticles of cobalt ferrite in polyaniline matrix in such a way that surface area of the rod-shaped polyaniline gets enhanced. Thermogravimetric analysis has been employed for measuring decomposition temperature of samples. Optical band gap of polyaniline is found to reduce from 1.63 to 1.49 eV due to embedment of cobalt ferrite nanoparticles. Cole-Cole plots fitted with two sub circuits is showing grain boundary like structure of synthesized samples. Conducting attributes of PANI/Cobalt ferrite composites have been studied in detail w.r.t. frequency. Magnetic properties at ± 10 KOe established the magnetic attributes in composites due to inclusion of ferrite particles. The electrochemical studies done over scan rate from 2 to 10 mV/s, of prepared materials for specific capacitance were found to be significantly high for composites as compare to pure conducting polyaniline or ferrites. This study promotes the synthesized materials as new opportunities for the energy storage devices.

Keywords Conducting polymers · Nanocomposites · Electric properties · Spinel ferrites · Energy storage

1 Introduction

Conducting polymers are the materials of interest for researchers in contemporary times. Their electrical and physical properties have made them important with respect to many applications. Regular development proved them useful in applications like electromagnetic shielding, flexible LEDs etc [1–4]. Although considerable amount of work has been reported on conducting polymers, the conduction mechanism is yet not clear. It can be understood by looking at its internal arrangement. Electric properties of PANI

depends upon the arrangement of chains. In addition, there are many other factors which alter the electrical behaviour of PANI i.e., synthesis process, surfactants used, temperature of synthesis etc. Also, PANI has negligible magnetic properties [5, 6].

Nanocomposites of conducting polymer and inorganic materials have resulted in enhanced electric and magnetic properties of the materials [2, 7]. One of the remarkable examples of nanocomposites is conducting polymers and ferrites nanocomposites. Many properties, specially, magnetic properties, of conducting polymers have been improved by blending it with ferrites [8, 9]. Although the electric resistivity of ferrites is generally high, they have very robust nature and generally possess good magnetic properties [10–12].

Further, conducting polymer and ferrite both are good materials for electrodes in pseudocapacitors [13]. Pseudocapacitors store chemical energy in form of redox reactions of electrochemically active materials and release it in the form of electric energy. Flexibility of polyaniline grab interest of researchers but found them very delicate and less sturdy to use [14]. Although ferrites have been studied for

✉ Rajni Shukla
Drrajnishukla.phy@dcrustm.org

¹ Deenbandhu Chotu Ram University of Science and Technology, Murthal 131039, India

² Guru Jambheshwar University of Science and Technology, Hisar 125001, India

³ Department of Physics, National Institute of Technology, Kurukshetra 136119, India

the same application but it has its own limitations such as high recombination rate, resistivity and leakage current [15, 16]. Introducing ferrites into a matrix of conducting polypyrrole may overcome these limitations and make them more useful material for electrodes with more robustness. A very few studies have considered electric, magnetic and electrochemical properties of these composites simultaneously. For example, Prasanna et al. and Tanriverdi et al. [17, 18] studied electric properties upto 10 MHz frequency. Present study aims to explore the application of fabricated electrodes of composites in a battery or a pseudocapacitor using electrochemical activity. Also, electric properties of composites of polyaniline and cobalt ferrite have been studied using electric circuit fitting and the role of ferrite nanoparticles in the conductivity of composites have been highlighted.

The pure PANI, cobalt ferrite (CF) and their nanocomposites were prepared using in-situ chemical polymerization for composite and co precipitation for cobalt ferrite respectively. The nanocomposites series have increasing weight% of cobalt ferrite from 0.5%, 2.5%, 5% and 7.5% and they are named as HCP1, HCP2, HCP3 and HCP4 respectively for future references. Detailed analysis of structural, electrical, thermal, magnetic and electrochemical properties of PANI and its composites have been done to observe their electrochemical behaviour.

2 Synthesis of Materials

2.1 Materials Used

Cobalt nitrate (Merk), ferric nitrate (Merk), distilled water, oleic acid and ammonia were used to synthesis ferrite. Ammonium per sulphate (APS), Hydrochloric acid and freshly distilled monomer aniline (sigma) were used to synthesis the pure PANI and composites.

2.2 Synthesis of Cobalt Ferrite

Two different solutions of cobalt nitrate and ferric nitrate are prepared respectively. After stirring of half hour at room temperature, cobalt nitrate solution was poured into the ferric nitrate solution and stirred again for half hour. Then temperature of the solution was raised upto 70 °C and 10 ml of oleic acid was added to the solution. After stirring of 1 h, the solution mixture was reduced by adding ammonia drop by drop until the pH raised to 12. Precipitates thus formed were dried at 400 °C and sintered at 500 °C for 2 h.

2.3 Synthesis of PANI and PANI/CF Composites

Two molar HCL solution was prepared and 2 ml of aniline was added into it. Mixture was stirred for 2 h then oxidised

by adding 50ml APS dropwise. Colour of reaction solution changes to dull yellow then green to dark bluish green. Occurrence of dark bluish green colour is an indication of formation of PANI. The mixture was then filtered and washed with distilled water and ethanol. Obtained paste was dried at 40 °C for 36 h and grinded to fine powder. To synthesis nanocomposites, CF is used as reinforcement and added in the reaction mixture of PANI after stirring aniline and HCl solution for 2 h. Then the similar to synthesis of PANI, solution was oxidised with APS and obtained precipitates were washed and dried.

3 Characterizations of Materials

XRD have been done in the range of angle 5°–70°, using powder X-ray diffractometer (Rigaku IV, Japan) to confirm the synthesis of materials as well as to dig structural analysis of the materials. Perkin–Elmer Frontier spectrometer was used for FTIR spectrum in the infrared range of 400–4000 cm⁻¹. Optical properties were studied using Defuse reflectance spectroscopy (DRS) attachment on UV Vis spectrometer (LAMBDA 750, Perkin Elmer). Thermo-gravimetric analysis (TGA) was done to analyse thermal stability of samples. Wyen Kerr impedance analyser was used to analyse AC conductivity and Impedance of all materials within the frequency range of 100 Hz–100 KHz. The magnetic properties of the materials were measured through Vibrating Sample Magnetometer (VSM) technique (Microsense EV-9). Electrochemical studies were done using CHI 760E three electrode electrochemical workstation to investigate Cyclic Voltammetry. Complete process from synthesis of powder samples to synthesis of electrodes is explained with help of Fig. 1.

4 X-ray Diffraction

The XRD data was obtained at the rate of 4° per minute in the range of 5°–70°. Characteristic peaks of HCl doped PANI were observed at 2θ = 8.9°, 15.1°, 25.5°, 27°, 30.3°, and a small peak at 36.6° [19, 20]. Trend of crystallinity was estimated indirectly by calculating resolution (R) of XRD peaks from Manjunathan's formula [21] as given below.

$$R = \frac{m_1 + 2m_2 + \dots + m_{n-1}}{h_1 + h_2 + \dots + h_n} \quad (1)$$

Where, m_1, m_2, m_{n-1} , are depth between the peaks and h_1, h_2, h_n are heights of the peaks. Obtained values of resolution are tabulated in Table no.1. The resolution thus calculated is inversely proportional to crystallinity [21] (see Fig. 2).

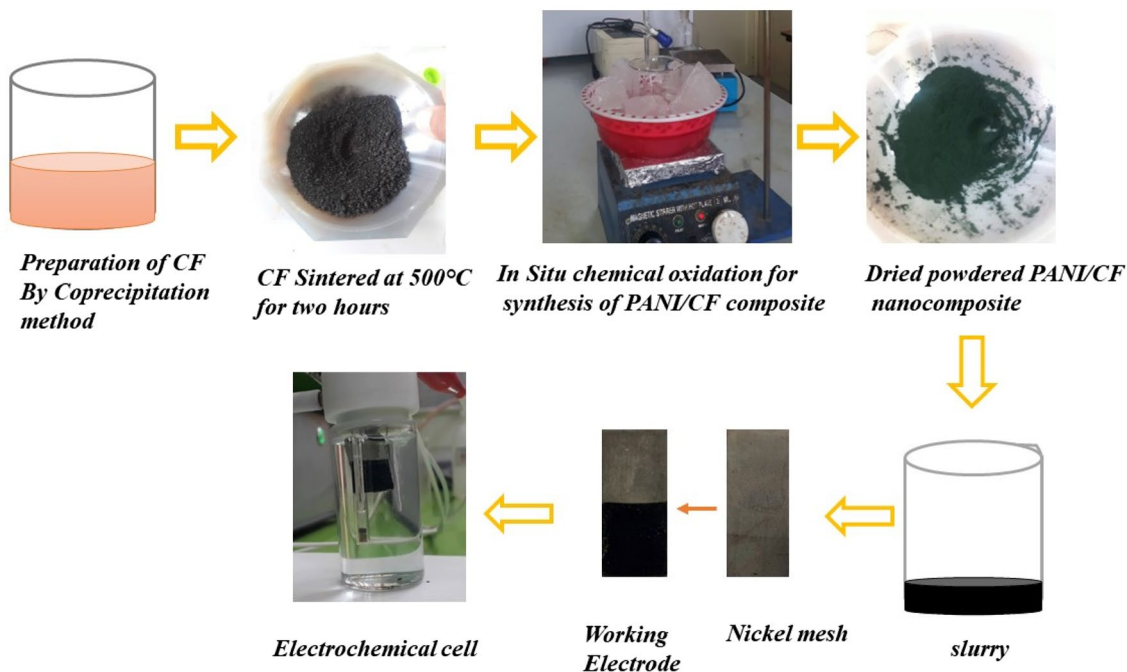


Fig. 1 Graphical representation synthesis of electrodes for electrochemical analysis

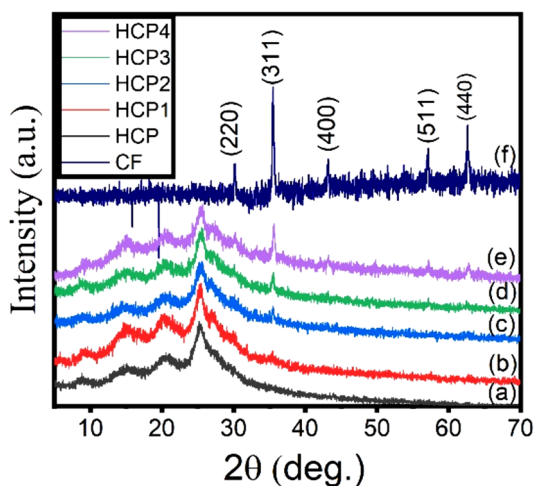


Fig. 2 XRD Spectra of **a** HCP, **b** HCP1, **c** HCP1, **d** HCP3, **e** HCP4 and **f** CF

Value of resolution can vary from zero for completely crystalline region to one for completely amorphous region. It was found that HCP4 have least resolution thus highest crystallinity as compared to other samples. It is also quoted earlier that polyaniline is semicrystalline in nature [22]. The characteristic peaks of spinel crystal structure of ferrites at 2θ value 30° , 35° , 43° , 53° , 57° , 63° is ascribed to the reflection planes of 220, 311, 222, 400, 422, 511, 440 respectively. The average crystallite size

(D) calculated from highest intensity peak (311), shown in Table 1, was estimated by Scherrer equation given as [23].

$$D = \frac{k\lambda}{\beta \cos\theta} \quad (2)$$

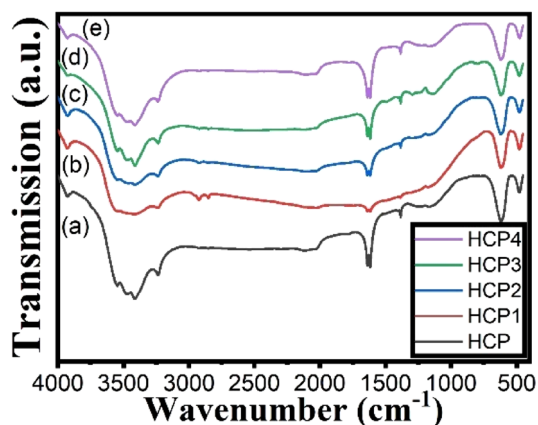
Where D is the average particle size, θ is the Bragg diffraction angle, β is the full width of the diffraction line at half the maximum intensity, λ is the wavelength and k (0.9) is a constant. Crystallite size is found to increase with increasing amount of CF i.e., from HCP1 to HCP4. This trend indicates increment of connectivity of ferrite NPs from HCP1 to HCP4. XRD results of composites show peaks of both PANI as well as ferrite together without any shift, implying successful synthesis of composites. Also increasing intensity of peak corresponding to (311) plane is due to increasing amount of cobalt ferrite [24].

5 FTIR

Fourier transform infrared spectroscopy (FTIR) is used to detect the information regarding bonding in the prepared samples (Fig. 3). It has been reported that in aniline oligomers and polymers, the region $3500\text{--}3100\text{ cm}^{-1}$ is because of N–H stretching. However, it may be of NH_2 or B–NH–B where B stands for Benzoid unit or terminal $\text{Q}=\text{NH}$ where Q stands for quinoid unit of PANI [25]. Major peaks of the samples are tabulated in Table 2. The peak at 2850 cm^{-1} is

Table 1 Resolution, crystallite size and optical band gap of HCP, HCP1, HCP1, HCP3, HCP4 and CF

Sample short name	Composition	Resolution (For the peaks corresponding to polymer phase)	Crystallite size(nm) (Calculated from (311) peak)	UV-Vis analysis	
				Position of peak 3 in KM function	Optical band gap (eV) (± 0.004)
HCP	PANI	0.974	–	638	1.63
HCP1	PANI@0.5%CF	0.963	5.79	634	1.64
HCP2	PANI@2.5%CF	0.980	13.52	651	1.44
HCP3	PANI@5%CF	0.977	19.45	637	1.60
HCP4	PANI@7.5%CF	0.870	22.08	596	1.49
CF	CF	–	30.89	–	2.17

**Fig. 3** FTIR spectra **a** HCP, **b** HCP1, **c** HCP2, **d** HCP3 and **e** HCP4

due to some minor impurities, hence not considered for analysis [26]. The spatial configuration of PANI chain can be estimated because trans arrangement of QBQ unit cause absorbance at 1380 cm^{-1} while cis configuration of QBQ give rise to 1315 cm^{-1} peak in FTIR spectra. Here all composites as well as pure PANI gives a peak at 1384 cm^{-1} so their backbone chain have trans arrangement of benzene rings [26]. Doublet at 1638 cm^{-1} and 1617 cm^{-1} corresponds

to conjugated C=C stretching [27]. As the benzene is substituted here, the absorption band near 600 cm^{-1} is due to out of plane bending of the ring. Further, metal-oxide bonds corresponding to ferrites also show low wave number band below 600 cm^{-1} .

6 Scanning Electron Microscopy

The SEM images of all samples were observed at 100 nm scale. Particles of pure polyaniline have elongated capsule like shape whereas cobalt ferrite particles appear spherical and grainy (Fig. 4a and b). In composites the spherical particles of CF covered the Capsule shaped particles of polyaniline. Also, in all composites CF particles are uniformly distributed causing agglomeration of PANI.

7 UV-Vis Spectroscopy

Basically, low energy band gaps were observed in doped conducting polymers [28]. Many theories like Su-Schrieffer Heeger model favours the fact that doping create polarons in polymers which results into formation of new energy bands

Table 2 FTIR transmission peaks of Polyaniline and the four composites

Related bonds	Peaks position of HCP	Peaks position of HCP1	Peaks position of HCP2	Peaks position of HCP3	Peaks position of HCP4	References
Out of plane bending of the benzene ring	619	619	619	619	619	
stretching of C–N bond of aromatic amine	1384	1384	1384	1384	1384	[26]
Doublet for conjugated C=C stretching	1617, 1638	1617, 1638	1617, 1638	1617, 638	1617, 1638	[27]
Stretching of C–H bond of Benzene ring	2852	2852	2854	2853	2852	[26]
N–H Bond stretching	3236	3235	3236	3236	3236	[25]

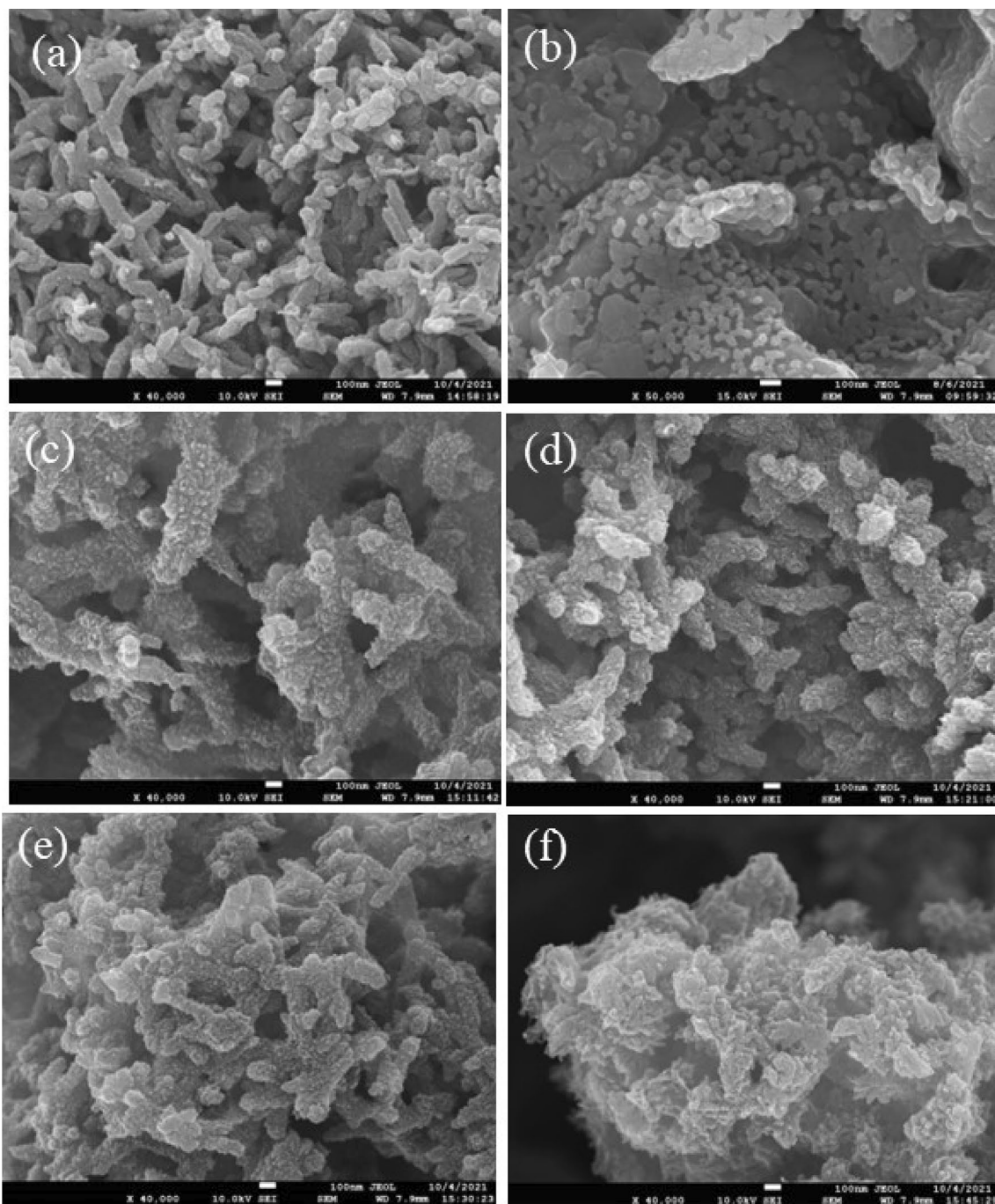


Fig. 4 SEM Images of **a** HCP (PANI), **b** CF and **c** HCP1, **d** HCP2, **e** HCP3, **f** HCP4 composites

in the otherwise forbidden region [29]. UV-Vis spectroscopy was done by Diffuse Reflectance Technique to know about these polaron bands and to measure the optical band gap of the prepared samples. Kubelka and Munk equation to convert reflectance data into absorption is given below [30]:

$$F(R) = \frac{(1 - R)^2}{2R} \quad (3)$$

Hence obtained UV-Vis absorption spectra of CF show a broad band from 350 to 600 nm as also reported in literature (Fig. 5 Inset). For PANI and PANI/CF composites three absorption bands are observed at 320–360 nm, 400–450 nm and 595–650 nm. First two bands are

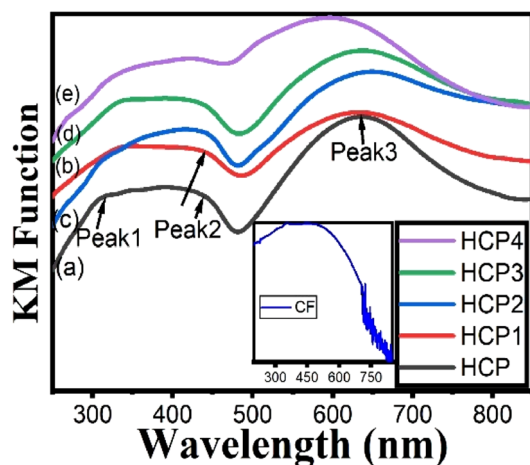


Fig. 5 KM function vs. wavelength for **a** HCP, **b** HCP1, **c** HCP2, **d** HCP3, **e** HCP4 and CF (inset)

amalgamated into a flat band. The peak1 and peak2 in Fig. 5 are attributed due to the $\pi-\pi^*$ transition of the benzenoid rings and π -polaron transitions respectively. Whereas, Peak 3 corresponds to polaron to π^* transition thus confirming the Cl doped emeraldine state of polyaniline in sample. Also, this peak show slight blue shift with increased amount of CF NPs which may be due to some sorts of interactions ferrite and PANI chains [31]. Kubelka Munk function is used to find out optical band gap using equation:

$$F(R)hv = k(hv - E_g)^{1/2} \quad (4)$$

where, hv is the photon energy, k is a constant, E_g is a characteristic energy which is termed as optical band gap. Intercept of the linear part of the curve on the x-axis gives the value of E_g (Fig. 6). Optical band gap of composites is found to be lower than the PANI as shown in Table 1.

8 Thermogravimetric Analysis

TGA is a technique in which variation in weight of a material is observed with respect to temperature in a controlled atmosphere. TGA thermograms of PANI and composites is shown in (Fig. 7). Thermal stability of PANI is not good but cobalt ferrite was found to be thermally stable. So, composites are expected to have high thermal stability as compared to PANI. It can be seen from TGA graphs (inset) that Cobalt ferrite degrade only 0.3% approximately upto 300 °C and then a sudden weight loss (0.5%) occurs between 300 and 400 °C. The first weight loss is attributed to solvent and humidity and second weight loss is due to degradation of surfactants like oleic acid etc. having boiling point near or

300 °C [32]. PANI and composites decompose in three different steps. First rapid weight loss from 30 to 120 °C is due to evaporation of water. This reflects hygroscopic nature of PANI [22]. Second weight loss is due to decomposition of the dopants. The temperature from which second weight loss started is called decomposition temperature and it tabulated for PANI and composites shown in Table 3. It has been found that the third weight loss started close to 300 °C and it is attributed to the degradation and decomposition of the backbone units of PANI. The degradation of polymeric backbone units leads to the generation of substituted aromatic fragments. It was found that higher the amount of cobalt ferrite higher the decomposition temperature of the sample. Thus, composites gain thermal stability with increasing amount of cobalt ferrite.

9 Impedance Spectroscopy

9.1 AC Conductivity

AC conductivity of PANI and its composites show linear behaviour (Fig. 8) at low frequency (100 Hz–10 kHz) and increase exponentially at higher frequencies (10 kHz–10 MHz). This is because at lower frequencies rate of change of polarity of applied electric field is low therefore, charge carriers take more time to transverse in a particular direction. But at higher frequencies polarity of applied field changes rapidly and the charge carries moves to and forth motion. This hoping of charge carrier is supported in both PANI as well as in Cobalt Ferrite. Hence AC conductivity increases at higher frequencies.

The PANI shows an increase in AC conductivity with increase in frequency but at slow rate as compare to PANI/CF composites. AC conductivity also increases with increase in the amount of CF nanoparticles (from HCP1 to HCP4) in the PANI/CF composites. It is found that the presence of CF-NPs in the PANI/CFs causes a drastic increment in the AC conductivity at high frequency which may be attributed to the enhanced electron hopping phenomenon. However, at low frequency ac conductivity of most of the composites is lower than PANI but at high frequency all composites have conductivity higher than PANI. This clearly indicates that ferrite ions dominate in ac conduction as their charged ions can easily exchange charge in localized sites. To transverse freely inside the material, charge carriers need to overcome the percolation threshold [33]. Therefore, at low frequency, higher amount of ferrite nanoparticles is needed to interconnect them with each other (to overcome percolation threshold) and create a continuous path.

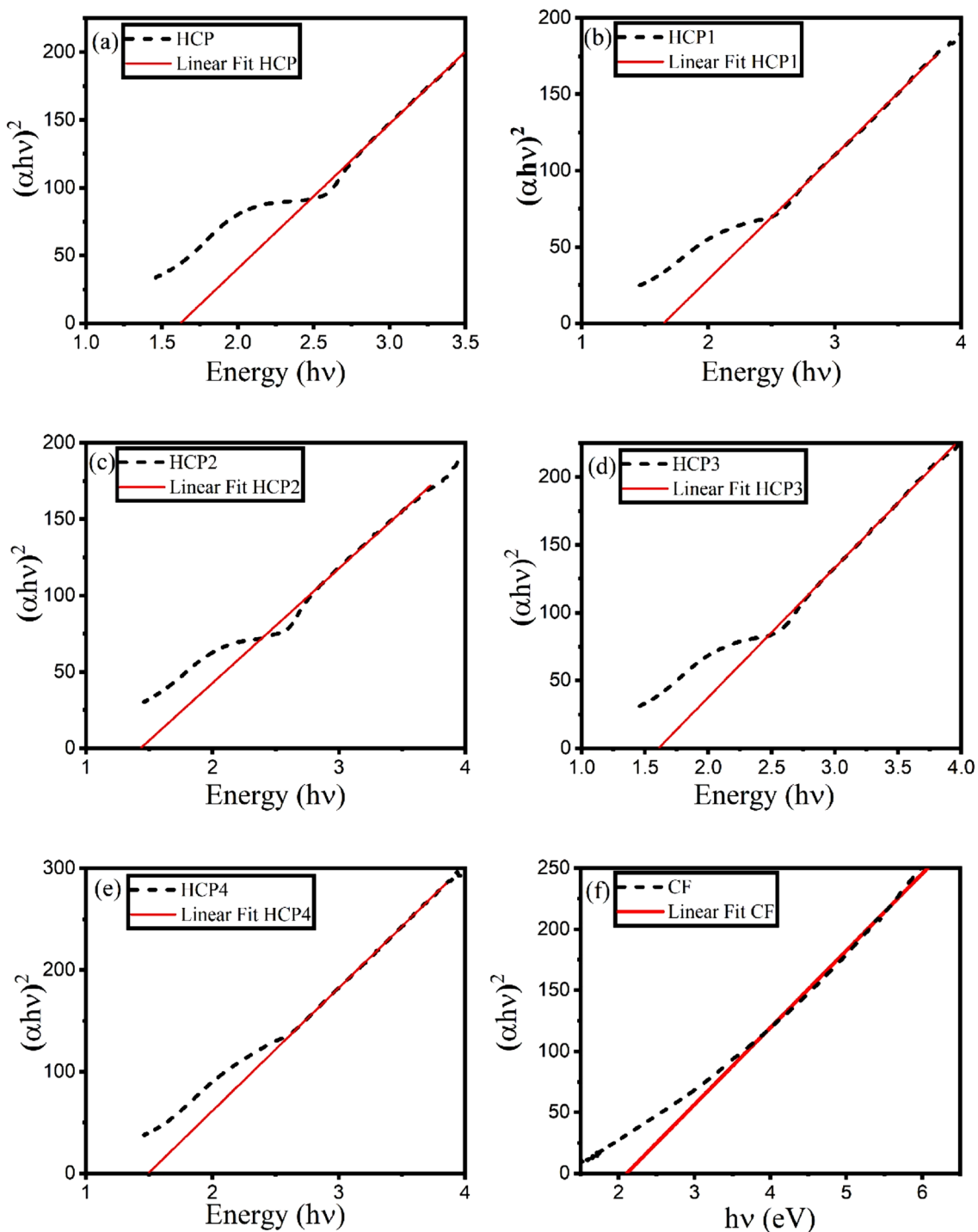


Fig. 6 Tauc plots of **a** HCP, **b** HCP1, **c** HCP1, **d** HCP3, **e** HCP4 and **f** CF

9.2 Cole–Cole

To study the mechanism of charge transitions into the materials Cole Cole plot have been used. It is a plot of real impedance against imaginary impedance of materials obtained from impedance spectroscopy. Arc of cole

cole plots (Fig. 9) of both polyaniline as well as PANI/CF composites seems to have centre below the x axis, and indicates the presence of more than one semicircle with poor resolution [34]. This is supported by fitted equivalent circuit which consists of two sub circuits (Fig. 9(b)). Each sub circuit contains one resistor named as R1 and

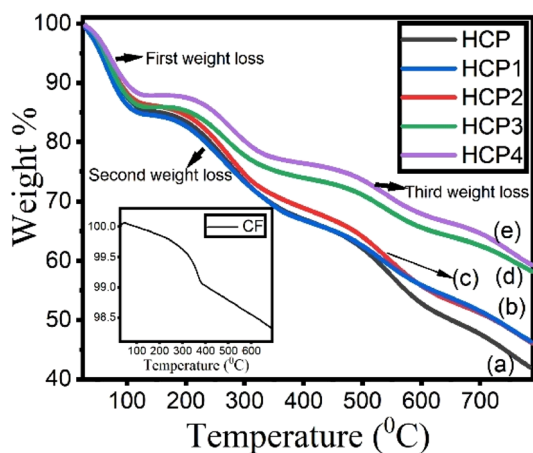


Fig. 7 Thermographs of **a** HCP, **b** HCP1, **c** HCP1, **d** HCP3, **e** HCP4 and CF (Inset)

Table 3 Decomposition temperature and final residue of polyaniline and composites obtained from TGA

Sample name	Decomposition temp. (°C)	Final residue wt%
HCP	266	42
HCP1	265	45
HCP2	268	46
HCP3	272	55
HCP4	277	59
CF	–	98

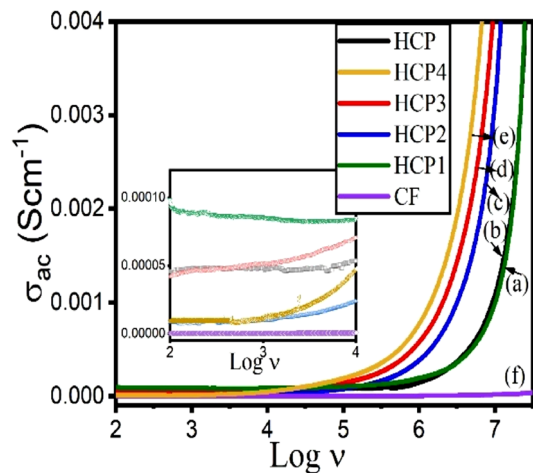


Fig. 8 AC conductivity of **a** HCP, **b** HCP1, **c** HCP2, **d** HCP3, **e** HCP4 and **f** CF in the frequency range 100 Hz–100 MHz (Inset Zoom in frequency range: 100 Hz–10 kHz)

R2, representing bulk resistance of the materials. First sub circuit has capacitor (C1) and second have constant phase element (CPE1). Values of each parameter have been mentioned in Table 4. These components represents space charge accumulation on electrodes and grain boundaries. Thus, grain and grain boundaries both are active in PANI and PANI/CF composites [35]. This also support the suggested reason behind the AC conductivity variation in the studied materials. Further, radius of semicircular arcs decreasing gradually from HCP to HCP4, indicating enhanced conductivity of composites. The Cole Cole plot of all the samples are found to fit well in the circuit shown in Fig. 8.

Further, for the confirmations and predictions of curve fitting and to distinguish two type of conduction mechanisms (long and short range) imaginary parts of different dielectric functions i.e., Z'' , M'' and $\tan\delta$ have been plotted. Overlapping of Z'' and M'' peaks imply pure long range conductivity mechanism e.g. in HCP3 (Fig. 10c), while separation between above said peaks imply mixed conduction mechanism, Fig. 10a,b [36]. Thus, Samples are moving from mixed to pure long range conductivity mechanism as the amount of CF is increased from HCP(0%) to HCP4(7.5%).

Tangent losses are high at high frequencies (Fig. 11) because of lack of synergy between polarity of applied field and induced dipoles in the samples. The losses of composites are higher at lower frequencies as compare to PANI and vice versa at higher frequency. This fact can be combined with their conductivity behaviour.

10 VSM

The magnetic properties of CoFe_2O_4 and $\text{CoFe}_2\text{O}_4/\text{PANI}$ composites were measured by vibrating sample magnetometer at room temperature (Fig. 12). The measured value of retentivity (M_r), coercivity (H_c) and saturation magnetisation (M_s) are tabulated in Table 5. As obvious CF have highest retentivity and saturation magnetization due to high magnetic moments of Cobalt ions. PANI have negligible retentivity as compared to CF. As the fraction of CF in composites increasing, retentivity also increases. Both M_s also shows linear increase with increasing amount of ferrite in the composites. This is due to the increase of magnetic domains and consequently increasing number of total spin moments which contribute to the values of M_s and M_r .

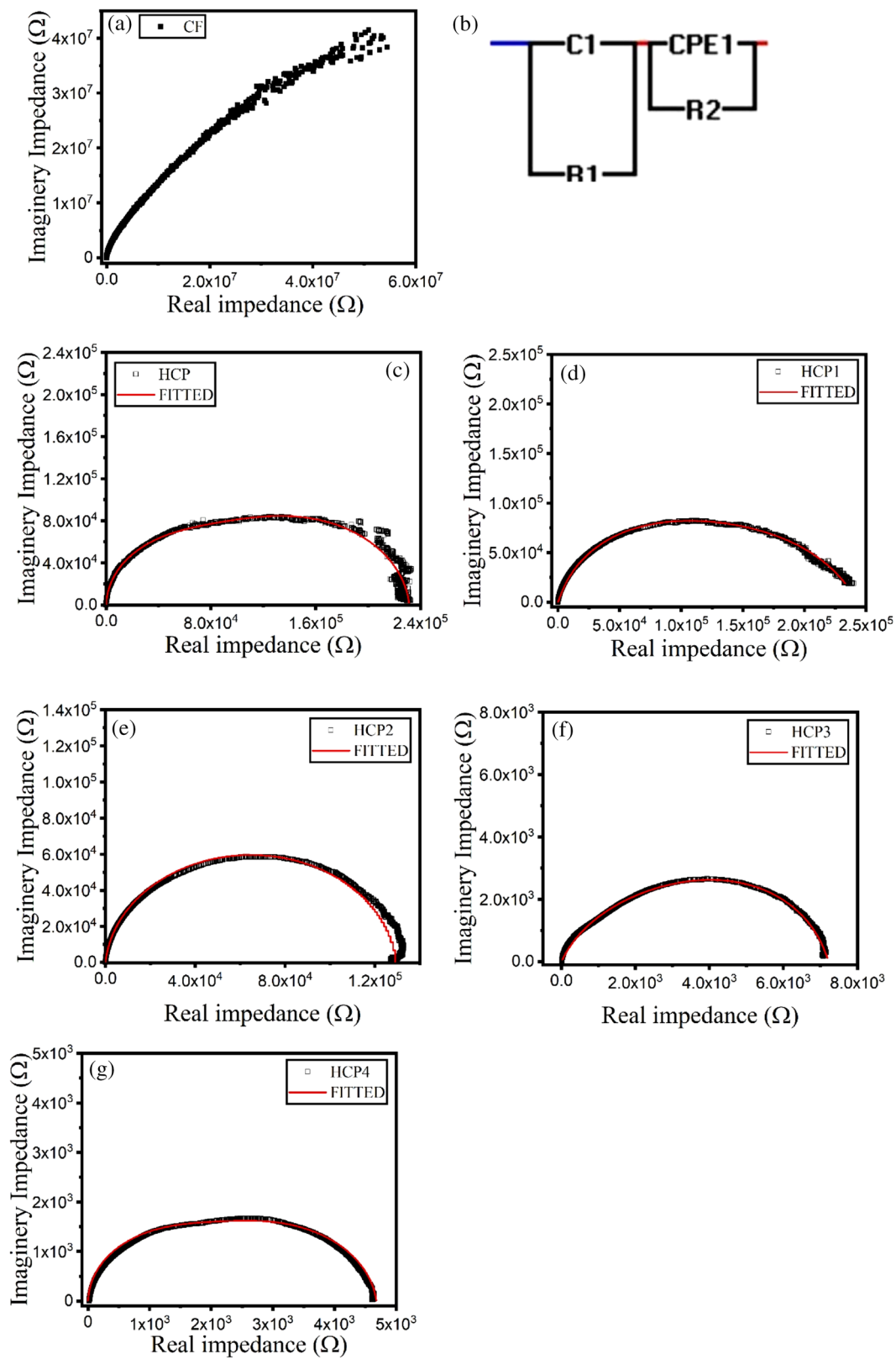
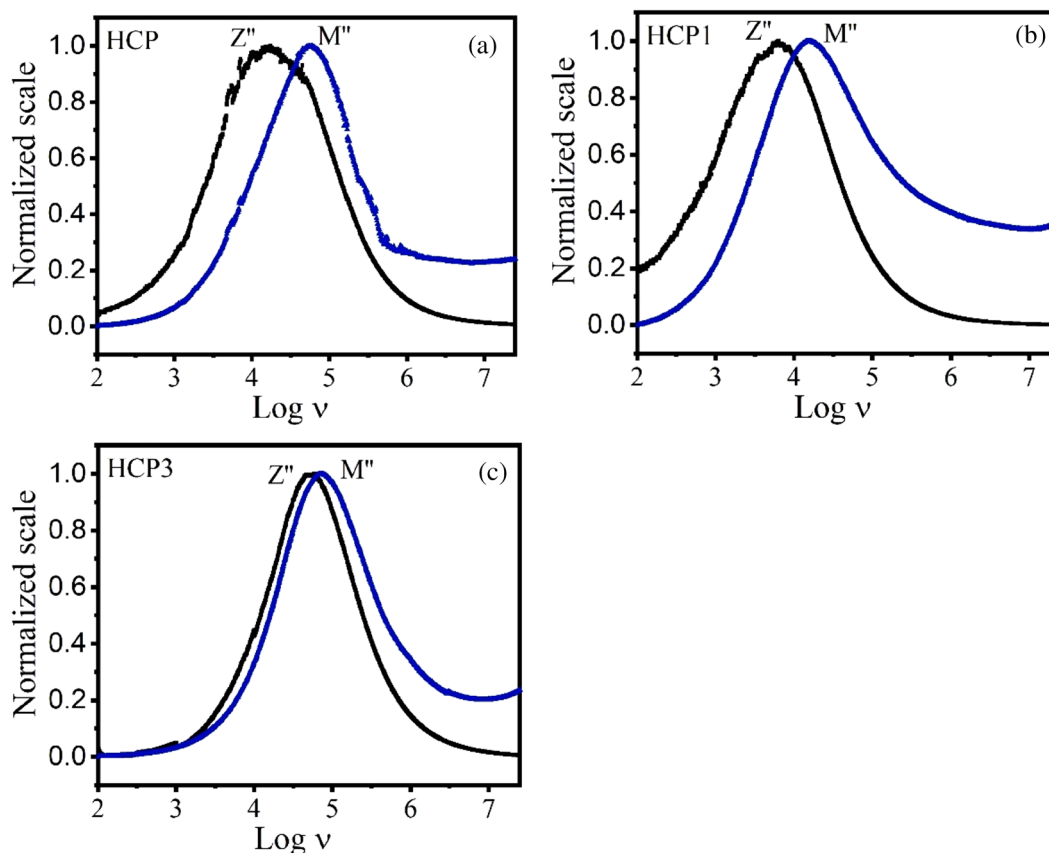


Fig. 9 Nyquist plot of a CF, b Fitted circuit to Nyquist plot of c HCP, d HCP1, e HCP2, f HCP3, g HCP4

Table 4 Grain, grain boundary parameters of HCP, HCP1, HCP2, HCP3 and HCP4 obtained from fitting

Parameters	HCP	HCP1	HCP2	HCP3	HCP4
R1	80,484	66,294	20,397	2422	1900
R2	1.5089×10^5	1.7632×10^5	1.341×10^5	4801	2680
C1	3.09×10^{-10}	1.98×10^{-10}	4.5×10^{-5}	5.03×10^{-10}	4.94×10^{-10}
P1	1.74×10^{-10}	3.09×10^{-10}	5.91×10^{-11}	3.53×10^{-10}	3.75×10^{-9}
n	0.9459	0.7552	0.9219	0.7519	0.9463

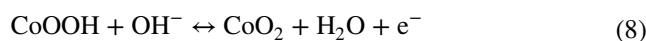
**Fig. 10** Log ν vs. imaginary Z'' and M'' for **a** HCP, **b** HCP1, **c** HCP3

11 Electrochemistry

Three electrode electrochemical workstation (CHI 760E) was used to obtain Cyclic voltammetry (CV) measurements. Out of the used three electrode one is the working electrode of the sample prepared. Second is the reference electrode for the measurement of potential of working electrode and it is made of Ag/AgCl. Third one is counter electrode which is a platinum wire. Considering its high ionic conductivity and low solvated ionic radius, 2M Potassium hydroxide was used as electrolyte. In this OH^- donating electrolyte the process of doping (Eq. 5) and dedoping (Eq. 6) of PANI are as follow



When oxidation occurs, ions get transferred to PANI backbone chain and ions get released from PANI into electrolyte during reduction. And similar redox reactions for Cobalt ferrite are as follow.



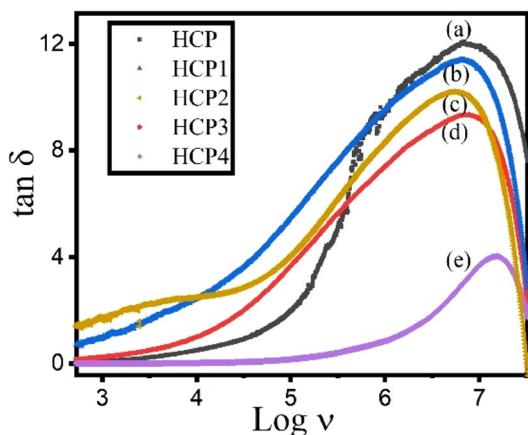


Fig. 11 Tangent loss of a HCP, b HCP1, c HCP2, d HCP3 and e HCP4

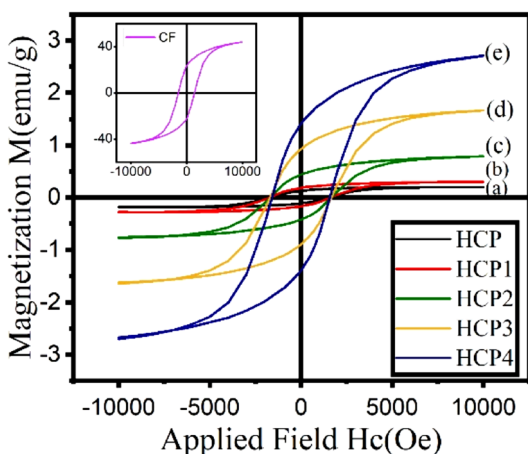
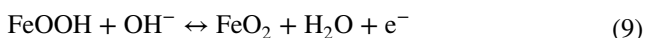


Fig. 12 Hysteresis loop for a HCP, b HCP1, c HCP1, d HCP3, e HCP4 and CF (inset)

Table 5 Coercivity and retentivity of polyaniline (HCP), CF and their composites

Samples	Ms (emu/g)	Hc (Oe)	Mr (emu/g)
HCP	0.18	1553	0.13
HCP1	0.28	1640	0.18
HCP2	0.74	1663	0.43
HCP3	1.66	1664	0.92
HCP4	2.55	1580	1.41
CF	44.04	1464	23



The CV curves corresponding to HCP, HCP1, HCP4 and CF samples at different scan rates (2, 4, 6, 8, 10 mV/s) are shown in Fig. 13. Potential window was taken in between 0.0 V and 0.5 V. Occurrence of sharp peaks of current is due to redox reactions taking place in the system on working electrode. And this current can be resolved into two parts. One is current due to diffusion and other is current due to fast faradaic reactions on the surface of the electrode.

$$i = i_{\text{diff}} + i_{\text{surf}} \tag{10}$$

And this total current is related to scan rate as follow:

$$I = av^b \tag{11}$$

Where v is scan rate, a and b are adjustable parameters depending upon properties of electrode material. b value actually compares the rate of change of current with changing potential. If current fails to maintain its reverberance with potential it means diffusion process is involved which is causing lag of current. Thus, value of $b=0.5$ is for battery and $b=1.0$ is for pseudocapacitors and any value between 0.5 and 1.0 corresponds to transition region between battery type material and pseudocapacitive material [37]. Calculated values of b for anodic current, cathodic current and average of b is tabulated in Table 6. The value of b shift towards 1.0 for composites, thus, it represents decrement in diffusion current of PANI after adding CF into it. Thus, CF support pseudocapacitor type behaviour of PANI.

The behaviour of electrode can be further evaluated by observing the separation of anodic and cathodic peaks along the potential axis (δE_{ac}) and shifting of current peaks. Large values of δE_{ac} (Table 7) and its variation with scan rate gives poor reversibility. Cobalt ferrite have largest value of δE_{ac} due to high recombination rates of ions. But nanocomposites have low values of δE_{ac} , thereby again supporting that composite have better capacitive type behaviour as compared to PANI. Specific capacitance was calculated from CV using (Eq. 12) and is 57, 61 and 66 F/g, for HCP, HCP1 and HCP4 respectively.

$$C_a = \frac{A}{2mvV} \tag{12}$$

where C_s , m , v , ΔV , and A are the specific capacitance (F/g), active mass (mg), scan rate (mV/s), potential window (V), and the area under the curve, respectively. Results are in consent with b values and δE_{ac} values. Change in surface morphology, enhanced conductivity strengthen the capacitive behaviour of PANI [38, 39].

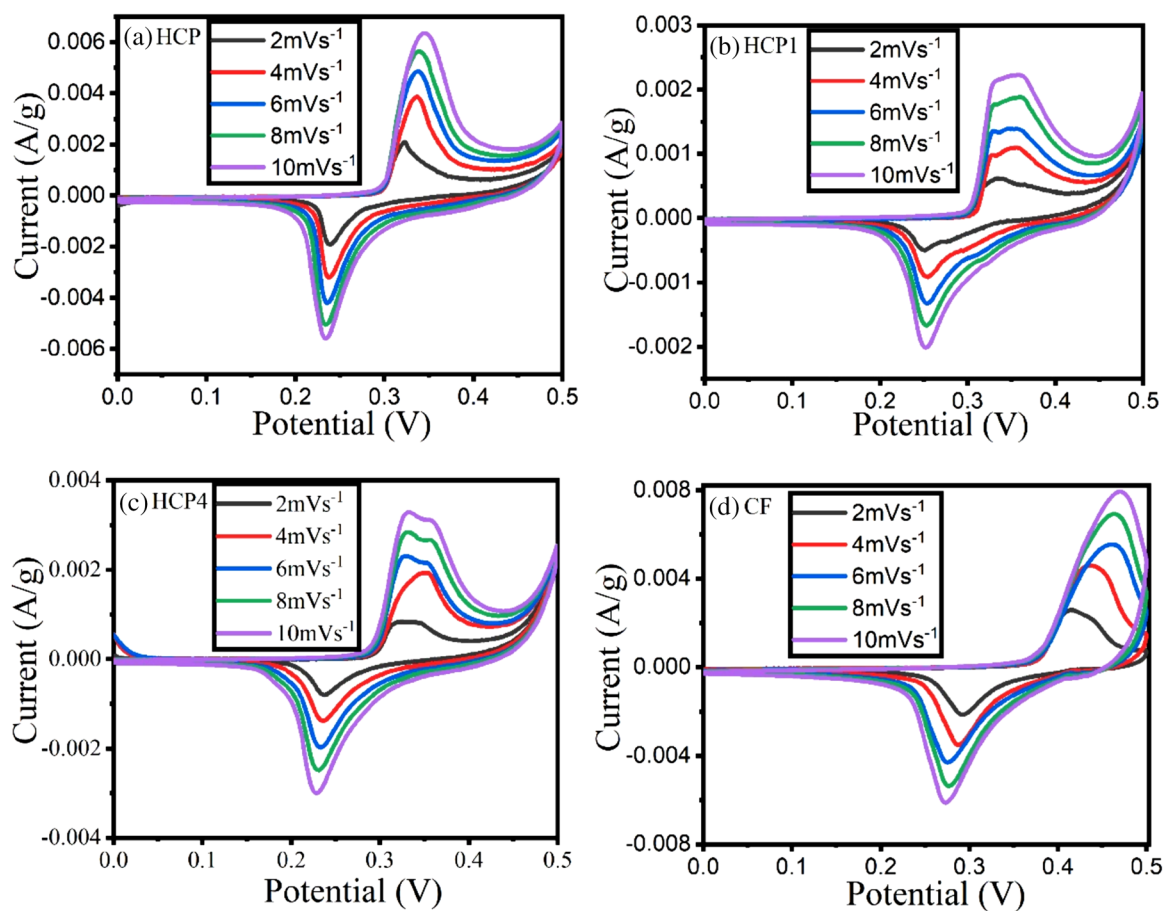


Fig. 13 Current vs. Voltage Plots for **a** HCP, **b** HCP1 and **c** HCP4

Table 6 b Values for HCP, HCP1 and HCP4

Sample	b Anodic	b Cathodic	Average b
HCP	0.68	0.68	0.68
HCP1	0.791	0.802	0.796
HCP4	0.828	0.822	0.825
CF	0.688	0.647	0.667

Table 7 δE_{ac} values for HCP, HCP1 and HCP4 for different scan rates ($v=2-10$)

Sample	δE_{ac} ($v=2$)	δE_{ac} ($v=4$)	δE_{ac} ($v=6$)	δE_{ac} ($v=8$)	δE_{ac} ($v=10$)	Average δE_{ac}
HCP	0.085	0.098	0.101	0.105	0.111	0.100
HCP1	0.082	0.081	0.076	0.079	0.080	0.0796
HCP4	0.096	0.096	0.096	0.101	0.104	0.09925

12 Conclusion

Spinel ferrite based PANI nanocomposites were successfully synthesised by In situ polymerization method. PANI is well supported by Cobalt ferrite with respect to its thermal, optical, magnetic and electric properties. This is due to reforms in morphology of the polymer and addition of spin particles after embedding ferrite into it. Optical energy

band gap of HCP4 is reduced upto 1.44 eV and 17% increase in final residues was observed in TGA. Conductivity of the nanocomposite with highest amount of ferrite is found to be highest of all samples. The nanocomposites showed the highest specific capacitance of 66Fg^{-1} obtained in potassium hydroxide solution at a 2 mV/s scan rate. Depending on electrochemical performance, nanocomposites are useful as electrode materials in pseudocapacitor.

Acknowledgment Authors are thankful to FIST Lab, department of physics, DCRUST for providing UV–Visible spectroscopy facility and Material Research Centre, MNIT Jaipur for Impedance spectroscopy.

Author Contributions S: Implementation of the research scheme, conceptualization, manuscript writing. MS and A: Data analysis and article review. RS: Supervision, review and edit the article. V: Data acquisition and formal analysis. PC: provided support for Electrochemical study, review and edit the article. The final manuscript has been read and approved by all authors.

Funding Author Anupama would like to thank the financial support from University Grant Commission (UGC) and is gratefully acknowledged for JRF-NET fellowship with F.No.: 16-6(DEC. 2017)/2018(NET/CSIR). Author Vikram gratefully acknowledge UGC for JRF-NET fellowship with F.No. 101/(CSIR-UGC NET JUNE 2019).

Declarations

Conflict of interest Authors declare that they do not have any conflict of interest.

References

- M. Saini, R. Shukla, S.K. Singh, Nickel doped cobalt ferrite/poly(Ani-co-Py) multiphase nanocomposite for EMI shielding application. *J. Inorg. Organomet. Polym. Mater.* (2019). <https://doi.org/10.1007/s10904-019-01163-7>
- X. Guo, A. Facchetti, The journey of conducting polymers from discovery to application. *Nat. Mater.* **19**(9), 922–928 (2020). <https://doi.org/10.1038/s41563-020-0778-5>
- F.Z. Hammadi, M.S. Belardja, M. Lafjah, A. Benyoucef, Studies of influence of ZrO₂ nanoparticles on reinforced conducting polymer and their optical, thermal and electrochemical properties. *J. Inorg. Organomet. Polym. Mater.* **31**(3), 1176–1184 (2021). <https://doi.org/10.1007/s10904-020-01730-3>
- A. Olad, M. Bastanian, H.B.K. Hagh, Thermodynamic and kinetic studies of removal process of hexavalent chromium ions from water by using bio-conducting starch–montmorillonite/polyaniline nanocomposite. *J. Inorg. Organomet. Polym. Mater.* **29**(6), 1916–1926 (2019). <https://doi.org/10.1007/s10904-019-01152-w>
- O. Chauvet et al., Magnetic and transport properties of polypyrrole doped with polyanions. *Synth. Met.* **63**(2), 115–119 (1994).
- C. Fite, Y. Cao, A.J. Heeger, Magnetic susceptibility of crystalline polyaniline. *Solid State Commun.* **70**(3), 245–247 (1989). [https://doi.org/10.1016/0038-1098\(89\)90319-0](https://doi.org/10.1016/0038-1098(89)90319-0)
- A.H. Abdalsalam, A.A. Ati, A. Abduljabbar, T.A. Hussein, structural, optical, electrical and magnetic studies of PANI/ferrite nanocomposites synthesized by PLD technique. *J. Inorg. Organomet. Polym. Mater.* **29**(4), 1084–1093 (2019). <https://doi.org/10.1007/s10904-018-0997-2>
- M. Swati, Saini, Anupama, R. Shukla, Investigation of structural, thermal, and electrical properties of magnesium substituted cobalt ferrite reinforced polyaniline nanocomposites. *Ceram. Int.* **47**(23), 33835–33842 (2021). <https://doi.org/10.1016/j.ceramint.2021.08.295>
- R. Megha, Y.T. Ravikiran, S.C. Vijaya Kumari, S. Thomas, “Influence of n-type nickel ferrite in enhancing the AC conductivity of optimized polyaniline–nickel ferrite nanocomposite”. *Appl. Phys. A Mater. Sci. Process.* **123**(4), 0 (2017). doi:<https://doi.org/10.1007/s00339-017-0866-9>
- R. Sharma, P. Pahuja, R.P. Tandon, Structural, dielectric, ferromagnetic, ferroelectric and ac conductivity studies of the BaTiO₃-CoFe_{1.8}Zn_{0.2}O₄ multiferroic particulate composites. *Ceram. Int.* **40**(7 Part A), 9027–9036 (2014)
- L.G. Van Uitert, Dielectric properties of and conductivity in ferrites. *Proc. IRE* **44**(10), 1294–1303 (1956). <https://doi.org/10.1109/JRPROC.1956.274952>
- V.A.M. Brabers, Chapter 3 progress in spinel ferrite research. *Handb. Magn. Mater.* **8**, 189–324 (1995). [https://doi.org/10.1016/S1567-2719\(05\)80032-0](https://doi.org/10.1016/S1567-2719(05)80032-0)
- S.K. Kandasamy, K. Kandasamy, Recent advances in electrochemical performances of graphene composite (graphene-polyaniline/polypyrrole/activated carbon/carbon nanotube) electrode materials for Supercapacitor: a review. *J. Inorg. Organomet. Polym. Mater.* **28**(3), 559–584 (2018). <https://doi.org/10.1007/s10904-018-0779-x>
- M. Hughes, G.Z. Chen, M.S.P. Shaffer, D.J. Fray, A.H. Windle, Controlling the nanostructure of electrochemically grown nanoporous composites of carbon nanotubes and conducting polymers. *Compos. Sci. Technol.* **64**(15), 2325–2331 (2004). <https://doi.org/10.1016/j.compscitech.2004.01.026>
- D.H. Deng et al., Fabrication of cobalt ferrite nanostructures and comparison of their electrochemical properties. *Cryst. Res. Technol.* **47**(10), 1032–1038 (2012). <https://doi.org/10.1002/crat.20120161>
- S.D. Raut, S. Sangale, R.S. Mane, *Ferrites in energy: limitations and perspectives* (Elsevier Inc., Amsterdam, 2020)
- G.D. Prasanna, H.S. Jayanna, In-situ synthesis, characterization and, frequency dependent AC conductivity of polyaniline/CoFe₂O₄ nanocomposites. *J. Adv. Dielectr.* **01**(03), 357–362 (2011). <https://doi.org/10.1142/S2010135X1100043410.1142/S2010135X11000434>
- E.E. Tanrıverdi, A.T. Uzumcu, H. Kavas, A. Demir, A. Baykal, Conductivity study of polyaniline-cobalt ferrite (PANI-CoFe₂O₄) nanocomposite. *Nano-Micro Lett.* **3**(2), 99–107 (2011). <https://doi.org/10.1007/bf03353658>
- M. Saini, S.K. Singh, R. Shukla, A. Kumar, Mg doped copper ferrite with polyaniline matrix core–shell ternary nanocomposite for electromagnetic interference shielding. *J. Inorg. Organomet. Polym. Mater.* **28**(6), 2306–2315 (2018). <https://doi.org/10.1007/s10904-018-0907-7>
- E.A. Sanches, J.C. Soares, A.C. Mafud, E.G.R. Fernandes, F.L. Leite, Y.P. Mascarenhas, Structural characterization of chloride salt of conducting polyaniline obtained by XRD, SAXD, SAXS and SEM. *J. Mol. Struct.* **1036**, 121–126 (2013). <https://doi.org/10.1016/j.molstruc.2012.09.084>
- B.R. Manjunath, A. Venkataraman, T. Stephen, The effect of moisture present in polymers on their X-ray diffraction patterns. *J. Appl. Polym. Sci.* **17**(4), 1091–1099 (1973). <https://doi.org/10.1002/app.1973.070170407>
- M. Das, A. Akbar, D. Sarkar, Investigation on dielectric properties of polyaniline (PANI) sulphonic acid (SA) composites prepared by interfacial polymerization. *Synth. Met.* **249**(October 2018), 69–80 (2019). <https://doi.org/10.1016/j.synthmet.2019.02.004>
- H.S. Mund, B.L. Ahuja, “Structural and magnetic properties of mg doped cobalt ferrite nano particles prepared by sol-gel method”.

- Mater. Res. Bull. **85**, 228–233 (2017). doi:<https://doi.org/10.1016/j.materresbull.2016.09.027>
24. M. Saini, R. Shukla, S.K. Singh, EMI shielding performance of Ni substituted cobalt ferrite loaded polypyrrole nanocomposites. Dae Solid State Phys. Symp. **2115**(July), 030092 (2019). <https://doi.org/10.1063/1.5112931>
 25. Y. Cao, S. Li, Z. Xue, D. Guo, “Spectroscopic and electrical characterization of some aniline oligomers and polyaniline”. Synth. Met. **16**(3), 305–315 (1986). doi:[https://doi.org/10.1016/0379-6779\(86\)90167-0](https://doi.org/10.1016/0379-6779(86)90167-0)
 26. W. Li-Xiang, J. Xia-Bin, W. Fo-Song, “Infrared spectra of soluble polyaniline”. Acta Chim. Sin English Ed. **7**(1), 53–58 (1989). doi:<https://doi.org/10.1002/cjoc.19890070108>
 27. R.M. Silvesterstein, F.X. Webster, D.J. Kiemle, *Spectrometric identification of organic compounds* (USA, Wiley, 2015)
 28. M. Wan, Absorption spectra of thin film of polyaniline. J. Polym. Sci. A Polym. Chem. **30**, 543–549 (1992)
 29. T.A. Skotheim, J.R. Reynolds, *Conjugated polymers theory, synthesis, properties and characterization* (CRC press, 2007)
 30. P. Makuła, M. Pacia, W. Macyk, How to correctly determine the band gap energy of modified semiconductor photocatalysts based on UV-Vis spectra. J. Phys. Chem. Lett. **9**(23), 6814–6817 (2018). <https://doi.org/10.1021/acs.jpcclett.8b02892>
 31. M. Khairy, Synthesis, characterization, magnetic and electrical properties of polyaniline/NiFe₂O₄ nanocomposite. Synth. Met. **189**, 34–41 (2014). <https://doi.org/10.1016/j.synthmet.2013.12.022>
 32. Z. Mahhouthi et al., Chemical synthesis and magnetic properties of monodisperse cobalt ferrite nanoparticles. J. Mater. Sci. Mater. Electron **30**(16), 14913–14922 (2019). <https://doi.org/10.1007/s10854-019-01863-3>
 33. G.C. Psarras, Hopping conductivity in polymer matrix-metal particles composites. Compos. A Appl. Sci. Manuf. **37**(10), 1545–1553 (2006). <https://doi.org/10.1016/j.compositesa.2005.11.004>
 34. G.W. Walter, A review of impedance plot methods used for corrosion performance analysis of painted metals. Corros. Sci. **26**(9), 681–703 (1986). [https://doi.org/10.1016/0010-938X\(86\)90033-8](https://doi.org/10.1016/0010-938X(86)90033-8)
 35. S. Dagar, A. Hooda, S. Khasa, M. Malik, Structural refinement, investigation of dielectric and magnetic properties of NBT doped BaFe₁₂O₁₉ novel composite system. J. Alloys Compd. (2020). <https://doi.org/10.1016/j.jallcom.2020.154214>
 36. R. Gerhardt, Impedance and dielectric revisited: distinguishing from long-range conductivity. J. Phys. Chem. Solids **55**(12), 1491–1506 (1995)
 37. M. Kaur, P. Chand, H. Anand, Effect of different synthesis methods on morphology and electrochemical behavior of spinel NiCo₂O₄ nanostructures as electrode material for energy storage application. Inorg. Chem. Commun. **134**, 108996 (2021). <https://doi.org/10.1016/j.inoche.2021.108996>
 38. H. Jiang, T. Zhao, J. Ma, C. Yan, C. Li, Ultrafine manganese dioxidenanowire network for high-performance supercapacitors. Chem. Commun. **47**(4), 1264–1266 (2011). <https://doi.org/10.1039/C0CC04134C>
 39. J. Liu et al., Advanced energy storage devices: basic principles, analytical methods, and rational materials design. Adv. Sci. **5**, 1 (2018). <https://doi.org/10.1002/advs.201700322>

Publisher's Note Springer Nature remains neutral with regard to jurisdictional claims in published maps and institutional affiliations.

Springer Nature or its licensor (e.g. a society or other partner) holds exclusive rights to this article under a publishing agreement with the author(s) or other rightsholder(s); author self-archiving of the accepted manuscript version of this article is solely governed by the terms of such publishing agreement and applicable law.